processes

MDPI

*Article*

# Equilibrium Biosorption of $Zn^{2+}$ and $Ni^{2+}$ Ions from Monometallic and Bimetallic Solutions by Crab Shell Biomass

**Liliana Morales-Barrera and Eliseo Cristiani-Urbina ***

Departamento de Ingeniería Bioquímica, Escuela Nacional de Ciencias Biológicas, Instituto Politécnico Nacional, Ciudad de México 11340, Mexico; lilianamor@prodigy.net.mx
* Correspondence: ecristiani@ipn.mx; Tel.: +52-55-57-29-60-00 (ext. 57835)

**Abstract:** This work explored the technical feasibility of using crab shell (CS) as a promising, low-cost biosorbent to individually and simultaneously remove $Zn^{2+}$ and $Ni^{2+}$ from aqueous solutions. It was found that in both monometallic and bimetallic systems, $Zn^{2+}$ and $Ni^{2+}$ biosorption by CS was strongly dependent on the solution pH, with the optimum biosorption occurring at a pH of 6.0 for both heavy metals. The obtained isotherms for $Zn^{2+}$ and $Ni^{2+}$ biosorption onto CS in monometallic and bimetallic systems demonstrated that CS has a higher affinity for $Zn^{2+}$ than for $Ni^{2+}$. The experimental equilibrium data for the bimetallic system revealed that when one heavy metal is present in the system, there is a decrease in the equilibrium biosorption capacity for the other heavy metal; therefore, the combined action of $Zn^{2+}$ and $Ni^{2+}$ was antagonistic. The Sips and Redlich–Peterson isotherm models best fitted the equilibrium biosorption data for $Zn^{2+}$ and $Ni^{2+}$ in the monometallic systems, while the modified Sips model best fitted the binary biosorption equilibrium data. DRIFTS analyses indicated that carbonate ion, chitin, and proteins are mainly involved in the biosorption of $Zn^{2+}$ and $Ni^{2+}$ by CS from aqueous solutions, as confirmed using a range of analytical techniques.

**Keywords:** biosorption; mono-component isotherm; multicomponent isotherm; crab shell; nickel; zinc; DRIFTS; SEM-EDX; XRF; CLSM



**Citation:** Morales-Barrera, L.; Cristiani-Urbina, E. Equilibrium Biosorption of $Zn^{2+}$ and $Ni^{2+}$ Ions from Monometallic and Bimetallic Solutions by Crab Shell Biomass. *Processes* **2022**, *10*, 886. https://doi.org/10.3390/pr10050886

Academic Editor: Tao Sun

Received: 4 April 2022
Accepted: 27 April 2022
Published: 29 April 2022



## 1. Introduction

Divalent zinc ($Zn^{2+}$) and nickel ($Ni^{2+}$) are essential trace elements for many living organisms, and they play crucial roles in several biological metabolic processes; however, these heavy metals are also toxic at high levels [1]. Both $Zn^{2+}$ and $Ni^{2+}$ ions are commonly found in effluents discharged by anthropogenic activities and industry, including those based on mineral processing, the use of non-ferrous metals, galvanization, paint formulation, battery manufacture, and porcelain enameling, among others [2,3]. Due to the high $Zn^{2+}$ and $Ni^{2+}$ concentrations present in these effluents, they can impart deleterious effects on the environment and on living organisms [3–5]. More specifically, $Ni^{2+}$ can produce a wide variety of acute and chronic health effects in humans, such as lung and kidney damage, skin dermatitis, nausea, vomiting, diarrhea, dizziness, cyanosis, rapid respiration, chest pain, and extreme weakness [6,7]. In addition, $Ni^{2+}$ is an embryotoxic, teratogenic [6], carcinogenic, and nephrotoxic agent [8]. Although $Zn^{2+}$ is comparatively less toxic than several other heavy metal ions, prolonged exposure to high $Zn^{2+}$ concentrations can cause abdominal pain, nausea, vomiting, fatigue, lethargy, anemia, dizziness, focal neuronal deficits, diarrhea, and prostate cancer [9,10]. It has also been reported that binary mixtures of $Zn^{2+}$ and $Ni^{2+}$ ions can exhibit synergistic or additive adverse effects on biochemical and physiological processes in living organisms, and their toxic effects are therefore higher than anticipated based on the effect of single metal ions in a mixture [1]. Due to such toxic effects, the World Health Organization (WHO) has established allowable limits of 0.07 and 3 mg/L for $Ni^{2+}$ and $Zn^{2+}$ ions in drinking water, respectively [11,12].

To safeguard human health, as well as the terrestrial and aquatic environments and the living organisms that live in them, the removal of $Zn^{2+}$ and $Ni^{2+}$ ions from domestic and industrial wastewaters is of particular importance. For this purpose, several physico-chemical treatment methods are available for the removal of these ions from industrial wastewaters, including chemical coagulation–flocculation, chemical precipitation, ion exchange, ultrafiltration, reverse osmosis, and electrochemical methods [13]. However, these methods tend to suffer from a number of disadvantages, including high costs, complexity, and/or the generation of hazardous wastes [14]. In contrast, the biosorption approach appears to be a more attractive and viable treatment technology for removing heavy metals from industrial wastewaters because of its ease of operation, simplicity of design, adaptability, flexibility, effectiveness, efficacy, efficiency, biosorbent regeneration, eco-friendliness, and insensitivity to toxic pollutants [15,16]. Thus, a vast array of biomaterials have been studied in terms of their abilities to remove heavy metals from single metal aqueous solutions, with examples including nonliving filamentous fungi, bacteria, yeasts, microalgae, and seaweed, in addition to agro-industrial, fishery, and forestry biowastes [17]. In contrast, few studies have been published regarding the simultaneous biosorption of several heavy metal ions from multi-metal solutions, even though it is well known that some industrial wastewaters contain various heavy metals at high concentrations [18]. This is of particular importance, since the presence of more than one heavy metal in industrial wastewater may hamper the biosorption process due to the fact that the different heavy metals may interact both with each other in solution and may also compete for the biosorption binding sites present on the biosorbent surface [19,20]. Thus, to understand the behaviors of multicomponent biosorption systems and to design reliable processes and equipment for the biosorptive removal of heavy metals from industrial wastewater, it is essential to understand the equilibrium isotherms of multicomponent systems [19,21].

In the above context, crab shell (CS) is an abundant biowaste that originates from the seafood industry, and its disposal in large quantities remains a significant issue. The ability to recycle this biowaste into useful resources is therefore of particular interest to find potential alternative uses for the discarded CS. For example, CS has the potential to be used as a viable, readily available, and economically-feasible biosorbent due to its ability to remove heavy metals and other types of inorganic and organic contaminants from wastewater systems [22]. More specifically, CS has been found to exhibit a remarkable ability to biosorb heavy metal ions from single and multicomponent aqueous solutions, such as those containing $Pb^{2+}$, $Cd^{2+}$, $Cr^{3+}$ [23], $Ni^{2+}$ [24], $V^{5+}$, $Cr^{6+}$ [25], $Cu^{2+}$ [26], $Zn^{2+}$, and $Mn^{2+}$ [27]. These efficient biosorbent properties of CS can be attributed to its mechanical resistance and its rigid structure [27], in addition to the fact that it possesses a wide variety of functional groups on its surface that are capable of biosorbing different heavy metals [22,28].

Thus, we herein report our investigation into the potential of CS to biosorb $Zn^{2+}$ and $Ni^{2+}$ ions from monometallic and bimetallic aqueous solutions. Furthermore, several isotherm models were studied in a comparative manner to evaluate their suitability for describing the CS biosorption behavior in both types of solution. Additionally, diffuse reflectance infrared Fourier transform spectroscopy (DRIFTS), X-ray fluorescence spectroscopy (XRF), scanning electron microscopy coupled with energy dispersive X-ray spectroscopy (SEM-EDX), and confocal laser scanning microscopy (CLSM) studies were performed to confirm the biosorption of $Zn^{2+}$ and $Ni^{2+}$ ions onto CS.

## 2. Materials and Methods

### 2.1. The Biosorbent

Samples of *Callinectes sapidus* crab, commonly known as blue crab, were acquired at a local market in Mexico City, Mexico. To separate the crab shells from the crabmeat, the crab samples were boiled at 92 °C for 15 min, washed exhaustively with deionized water, and subsequently dried at 65 °C until reaching a constant mass. The dried samples were then milled, and the resulting particles were sifted through standard sieves to harvest the

particle fraction with sizes ranging from 0.3 to 0.5 mm, which was used in the subsequent biosorption experiments.

### 2.2. Preparation of the $Zn^{2+}$ and $Ni^{2+}$ Aqueous Solutions

Stock solutions of 40 mM $Zn^{2+}$ and 40 mM $Ni^{2+}$ ions were prepared by weighing the appropriate quantity of $ZnSO_4 \cdot 7H_2O$ (>99.9%, JT Baker, Monterrey, Mexico) or $NiSO_4 \cdot 6H_2O$ (>99.1%, JT Baker, Monterrey, Mexico) and making up the volume to 1 L using deionized water. The stock $Zn^{2+}$ and $Ni^{2+}$ solutions were then appropriately diluted with deionized water to produce test solutions of the desired concentrations, which were used in the individual and simultaneous $Zn^{2+}$ and $Ni^{2+}$ biosorption experiments.

### 2.3. Biosorbent Characterization

We have characterized CS in terms of average specific surface area, total pore volume, and average pore diameter. These characteristics were determined from nitrogen adsorption–desorption isotherms at 77.35 K using a Quantachrome NovaWin gas sorption analyzer (Quantachrome Instruments, Boynton Beach, FL, USA). The CS particles were degassed with nitrogen at 373 K. Then, we determined the specific surface area of the CS using the Brunauer, Emmett, and Teller (BET) multipoint method, and the total pore volume and pore diameter by applying the Barrett, Joyner, and Halenda (BJH) method [16].

### 2.4. Single and Binary Metal Biosorption Studies

Previous kinetic studies performed using metal solutions of different pH values, with different initial $Zn^{2+}$ and $Ni^{2+}$ concentrations, and using CS as a biosorbent, showed that the biosorption times to reach equilibrium were less than 24 h [29]. Therefore, a CS/solution contact time of 24 h was employed for the equilibrium biosorption studies using the single or binary metal ion solutions. These studies were conducted using a 50 mL volume of the desired metal solution and a 1 g/L concentration of CS in a 250 mL Erlenmeyer flask under 180 rpm constant agitation at 25 °C. The pH values of the metal solutions were calibrated to the desired values using 0.1 M NaOH or HCl solutions.

To assess the effect of the solution pH on the individual biosorption of $Zn^{2+}$ and $Ni^{2+}$ by CS, solutions with initial metal concentrations of 2 mM and pH values ranging from 1.0 to 6.0 were used. The same pH range was also employed for the binary metal biosorption experiments, using equimolar initial concentrations of $Zn^{2+}$ and $Ni^{2+}$ (i.e., 2 mM). It should be noted that pH values > 6.0 were not examined to prevent $Zn(OH)_2$ and $Ni(OH)_2$ precipitation.

To examine the effects of the initial $Zn^{2+}$ and $Ni^{2+}$ concentrations on the equilibrium biosorption process for the two monometallic systems, the initial concentrations of the metal ions were varied within the range of 0.2–40 mM. For the binary metal system, an array of assays was performed by maintaining the initial concentration of one heavy metal constant within the 0.2–40 mM range, while varying the initial concentration of the other heavy metal within the same range.

Upon completion of the single and binary biosorption experiments, the Erlenmeyer flasks were removed from the water bath shaker, and the biosorbent and metal solution were separated by filtration through Whatman No. 42 filter paper. The residual $Zn^{2+}$ and/or $Ni^{2+}$ concentrations of the filtrates were measured according to the Zincon Method 8009 and the Dimethylglyoxime Method 10220, respectively, following the instructions outlined in the Hach Water Analysis Handbook [30].

Additionally, CS-free controls were also assayed at identical experimental conditions as those used for the $Zn^{2+}$ and/or $Ni^{2+}$ biosorption trials to ascertain the degree of $Zn^{2+}$ and/or $Ni^{2+}$ ion loss by adsorption onto the glass and/or by means of precipitation. It should be noted that no significant differences were detected in the $Zn^{2+}$ and/or $Ni^{2+}$ concentrations for the CS-free control experiments, thereby indicating that the removal of these metal ions could be attributed to the action of the CS biosorbent.

The biosorption capacities of the $Zn^{2+}$ and $Ni^{2+}$ ions at equilibrium ($q_e$, mmol/g) were estimated according to Equation (1):

$$q_e = \frac{C_i - C_e}{C_b} \quad (1)$$

where $C_e$ and $C_i$ are the equilibrium and initial concentrations of $Zn^{2+}$ or $Ni^{2+}$ in the aqueous solution (mmol/L), respectively, and $C_b$ is the CS concentration (g/L).

### *2.5. Biosorption Equilibrium Modeling of $Zn^{2+}$ and/or $Ni^{2+}$ Ions onto CS*

To gain a suitable understanding of the monometallic and bimetallic biosorption systems, the derivation of an accurate mathematical representation of the equilibrium biosorption isotherm is of paramount importance. More specifically, modeling of the equilibrium biosorption isotherm is necessary to derive design parameters that can be used for optimization and scaleup purposes, as well as to allow comparisons between the biosorption performances of different biosorption systems [31]. Additionally, these isotherm model parameters frequently provide valuable information regarding the interactions between the adsorbate and the biosorbent, the affinity of the biosorbent toward the adsorbate, and the surface characteristics of the biosorbent [32]. It is therefore crucial to identify the most suitable mathematical models to describe the equilibrium isotherms for the single and binary biosorption of $Zn^{2+}$ and $Ni^{2+}$ ions onto CS.

The equilibrium data for single $Zn^{2+}$ and $Ni^{2+}$ biosorption systems were analyzed using the Langmuir, Freundlich, Sips, and Redlich–Peterson isotherm models (Table 1), which have been extensively used to examine equilibrium data for wastewater treatment applications [17,33,34].

**Table 1.** Biosorption isotherm models for the single heavy metal systems.

| Model | Equation | | Nomenclature | Reference |
|---|---|---|---|---|
| Langmuir | $q_e = \frac{q_m b_L C_e}{1+b_L C_e}$ | $q_e$ | Equilibrium biosorption capacity (mmol/g) | [33] |
| | | $q_m$ | Maximum biosorption capacity (mmol/g) | |
| | | $C_e$ | Equilibrium heavy metal concentration in the aqueous phase (mM) | |
| | | $b_L$ | Langmuir constant (L/mmol) | |
| Freundlich | $q_e = k_F C_F^{\frac{1}{n_F}}$ | $1/n_F$ | Relative indicator of the biosorption intensity | [33] |
| | | $k_F$ | Indicator of the capacity of biosorption (mmol/g) $(mmol/L)^{-1/nF}$ | |
| Redlich–Peterson | $q_e = \frac{k_{RP} C_e}{1+(a_{RP} C_e{}^{b_{RP}})}$ | $k_{RP}$ | Model parameter (L/g) | [17] |
| | | $a_{RP}$ | Model parameter $(mmol/L)^{-BRP}$ | |
| | | $b_{RP}$ | Model parameter | |
| Sips | $q_e = \frac{q_m b_S C_e{}^{n_S}}{1+(b_S C_e{}^{n_S})}$ | $q_m$ | Maximum biosorption capacity (mmol/g) | [34] |
| | | $b_s$ | Model parameter $(mmol/L)^{-nS}$ | |
| | | $n_s$ | Sips parameter | |

Likewise, the nonmodified competitive Langmuir, uncompetitive Langmuir, partial competitive Langmuir, extended Freundlich, modified Sips, and modified Redlich–Peterson isotherm models were used in this work to fit the experimental data obtained for the simultaneous biosorption of $Zn^{2+}$ and $Ni^{2+}$ from bimetallic systems (Table 2) [20,35–38].

**Table 2.** Isotherm models used in this work for the binary biosorption of $Zn^{2+}$ and $Ni^{2+}$ by CS.

| Model | Equation | Nomenclature | Reference |
| --- | --- | --- | --- |
| Non-modified competitive Langmuir | $q_{eZn} = \frac{q_{mZn}{}' b_{LZn}{}' C_{eZn}}{1+b_{LNi}{}' C_{eNi}+b_{LZn}{}' C_{eZn}}$<br>$q_{eNi} = \frac{q_{mNi}{}' b_{LNi}{}' C_{eNi}}{1+b_{LNi}{}' C_{eNi}+b_{LZn}{}' C_{eZn}}$ | $q_{mZn}{}'$, $q_{mNi}{}'$: Maximum $Zn^{2+}$ and $Ni^{2+}$ biosorption capacity (mmol/g).<br>$b_{LZn}{}'$, $b_{LNi}{}'$: Langmuir constants for $Zn^{2+}$ and $Ni^{2+}$ biosorption (L/mmol)<br>$C_{eZn}$, $C_{eNi}$: Equilibrium $Zn^{2+}$ and $Ni^{2+}$ concentrations (mM). | [35] |
| Uncompetitive Langmuir | $q_{eZn} = \frac{q_{mZn}{}^{*}(b_{LZn}{}^{*} C_{eZn}+b^{*} C_{eZn}C_{eNi})}{1+b_{LNi}{}^{*} C_{eNi}+b_{LZn}{}^{*} C_{eZn}+b^{*} C_{eZn}C_{eNi}}$<br>$q_{eNi} = \frac{q_{mNi}{}^{*}(b_{LNi}{}^{*} C_{eNi}+b^{*} C_{eZn}C_{eNi})}{1+b_{LNi}{}^{*} C_{eNi}+b_{LZn}{}^{*} C_{eZn}+b^{*} C_{eZn}C_{eNi}}$ | $q_{mZn}{}^{*}$, $q_{mNi}{}^{*}$: Maximum $Zn^{2+}$ and $Ni^{2+}$ biosorption capacity (mmol/g).<br>$b_{LZn}{}^{*}$, $b_{LNi}{}^{*}$: Langmuir constants for $Zn^{2+}$ and $Ni^{2+}$ biosorption (L/mmol).<br>$b^{*}$: Langmuir parameter predicted by the uncompetitive model.<br>$C_{eZn}$, $C_{eNi}$: Equilibrium $Zn^{2+}$ and $Ni^{2+}$ concentrations (mM). | [36] |
| Partial competitive Langmuir | $q_{eZn} = \frac{q_{mZn}{}'' C_{eZn}\left(b''_{LZn}+b''_{LNi}b_{NiZn}C_{eNi}\right)}{1+b_{LZn}{}'' C_{eZn}+b_{LNi}{}'' C_{eNi}+\left(b''_{LZn}b_{ZnNi}C_{eZn}C_{eNi}+b''_{LNi}b_{NiZn}C_{eZn}C_{eNi}\right)}$<br>$q_{eNi} = \frac{q_{mNi}{}'' C_{eNi}\left(b''_{LNi}+b''_{LZn}b_{ZnNi}C_{eZn}\right)}{1+b_{LZn}{}'' C_{eZn}+b_{LNi}{}'' C_{eNi}+\left(b''_{LZn}b_{ZnNi}C_{eZn}C_{eNi}+b''_{LNi}b_{NiZn}C_{eZn}C_{eNi}\right)}$ | $q_{mZn}{}''$, $q_{mNi}{}''$: Maximum $Zn^{2+}$ and $Ni^{2+}$ biosorption capacity (mmol/g).<br>$b_{LZn}{}''$, $b_{LNi}{}''$: Langmuir constants for $Zn^{2+}$ and $Ni^{2+}$ biosorption (L/mmol).<br>$b_{NiZn}$, $b_{ZnNi}$: Affinity constant for $Ni^{2+}$ with the binding site already occupied by $Zn^{2+}$, and affinity constant for $Zn^{2+}$ with the binding site already occupied by $Ni^{2+}$, respectively. | [36] |
| Extended Freundlich | $q_{eZn} = \frac{k_{FZn}C_{eZn}\frac{1}{n_{FZn}}+x_{Zn}}{C_{eZn}{}^{x_{Zn}}+y_{Zn}C_{eNi}{}^{z_{Zn}}}$<br>$q_{eNi} = \frac{k_{FNi}C_{eNi}\frac{1}{n_{FNi}}+x_{Ni}}{C_{eNi}{}^{x_{Ni}}+y_{Ni}C_{eZn}{}^{z_{Ni}}}$ | $k_{FZn}$, $k_{FNi}$, $n_{FZn}$, $n_{FNi}$: Parameters derived from the corresponding single-component Freundlich isotherm.<br>$x_{Zn}$, $y_{Zn,}$ $z_{Zn,}$ $x_{Ni}$, $y_{Ni,}$ $z_{Ni}$: Freundlich parameters determined from the binary equilibrium data. | [37] |
| Modified Redlich–Peterson | $q_{eZn} = k_{RPZn}\frac{C_{eZn}}{\eta_{Zn}}\Big/\left[1+a_{RPZn}\left(\frac{C_{eZn}}{\eta_{Zn}}\right)^{b_{RPZn}}+a_{RPNi}\left(\frac{C_{eNi}}{\eta_{Ni}}\right)^{b_{RPNi}}\right]$<br>$q_{eNi} = k_{RPNi}\frac{C_{eNi}}{\eta_{Ni}}\Big/\left[1+a_{RPZn}\left(\frac{C_{eZn}}{\eta_{Zn}}\right)^{b_{RPZn}}+a_{RPNi}\left(\frac{C_{eNi}}{\eta_{Ni}}\right)^{b_{RPNi}}\right]$ | $\eta_{Zn,}$ $\eta_{\mathrm{Ni}}$: Correction coefficients for $Zn^{2+}$ and $Ni^{2+}$ ions estimated from binary equilibrium data.<br>$K_{RPNi}$, $K_{RPZn}$, $A_{RPNi}$, $A_{RPZ\mathrm{n}}$, $b_{RPNi}$, $b_{RPZN}$: Model parameters derived from the corresponding single-component biosorption data. | [38] |
| Modified Sips | $q_{eZn} = \frac{q_{msZn}{}' b_{sZn}{}' C_{eZn}{}^{n_{sZn}{}'}}{1+b_{sNi}{}' C_{eNi}{}^{n_{sNi}{}'}+b_{sZn}{}' C_{eZn}{}^{n_{sZn}{}'}}$<br>$q_{eNi} = \frac{q_{msNi}{}' b_{sNi}{}' C_{eNi}{}^{n_{sNi}{}'}}{1+b_{sNi}{}' C_{eNi}{}^{n_{sNi}{}'}+b_{sZn}C_{eZn}{}^{n_{sZn}{}'}}$ | $q_{msZn}{}'$, $q_{msNi}{}'$: Maximum $Zn^{2+}$ and $Ni^{2+}$ biosorption capacity (mmol/g).<br>$b_{sZn}{}'$, $b_{sNi}{}'$, $n_{sZn}{}'$, $n_{sNi}{}'$: Model parameters obtained from binary component biosorption data. | [20] |

### 2.6. Statistical Analyses and Determination of the Biosorption Isotherm Parameters

All batch equilibrium biosorption experiments were performed threefold to ensure the reproducibility and accuracy of the data. Mean values (calculated from triplicate experiments) ± standard deviations (SDs) are reported herein. The data obtained for the equilibrium biosorption of $Zn^{2+}$ and/or $Ni^{2+}$ were statistically examined by variance analysis with Tukey's assay and with a 95% confidence interval using SigmaStat V3.5 software (Systat Software, San Jose, CA, USA).

The Matlab V7.9 (The MathWorks Inc., Nattick, MA, USA) and SigmaStat V3.5 software programs were used to obtain the parameters for the monometallic and bimetallic isotherm models, respectively, through application of nonlinear regression analysis to the experimental equilibrium biosorption data. The goodness-of-fit of each isotherm model was evaluated using the determination coefficient ($R^2$), the root mean squared error (*RMSE*), and the sum of the squared errors (*SSE*). An $R^2$ value close to unity in addition to smaller *RMSE* and *SSE* values indicate a better description of the experimental biosorption data by an individual isotherm model.

### 2.7. Diffuse Reflectance Infrared Fourier Transform Spectroscopy (DRIFTS)

DRIFTS analysis was used to determine the CS surface functional groups responsible for the biosorption of $Zn^{2+}$ and/or $Ni^{2+}$ ions from aqueous solutions. More specifically, samples of CS (1 g/L) were added to monometallic solutions containing 20 mM $Zn^{2+}$ or $Ni^{2+}$, and to bimetallic solutions containing 20 mM of both $Zn^{2+}$ and $Ni^{2+}$. All solutions were at pH 6.0 and the CS/solution mixtures were agitated at 180 rpm for 24 h to saturate the biosorbent binding sites with the metal ions. Subsequently, the resulting suspensions were subjected to centrifugation at 4000 rpm for 4 min, and the CS pellets were washed exhaustively with deionized water to eliminate the unbound $Zn^{2+}$ and/or $Ni^{2+}$ ions. Centrifugation was then repeated (4000 rpm, 4 min) using the suspensions of CS pellets in deionized water to obtain pellets of the heavy metal-loaded CS, which were oven-dried to a constant weight at 105 °C.

Dried samples of the native CS (i.e., not loaded with heavy metal ions) and of the CS samples loaded with $Zn^{2+}$, $Ni^{2+}$, and $Zn^{2+}$+$Ni^{2+}$ ions were ground into fine powders using a mortar and pestle, mixed with KBr in a 1:5 ratio, and then analyzed by DRIFTS using a Perkin-Elmer diffuse reflectance device on a Perkin-Elmer Spectrum 2000 FTIR spectrometer (Perkin-Elmer, Inc., Waltham, MA, USA). DRIFTS spectra were collected over 64 scans in the wavenumber range of 4000–400 $cm^{-1}$ with a resolution of 4 $cm^{-1}$.

### 2.8. Scanning Electron Microscopy Combined with Energy Dispersive X-ray Spectroscopy (SEM-EDX)

SEM-EDX analysis was used to examine any changes in the elemental composition of the CS surface resulting from the biosorption of $Zn^{2+}$ and/or $Ni^{2+}$ ions. For this purpose, dried samples of the native CS, $Zn^{2+}$-loaded CS, $Ni^{2+}$-loaded CS, and $Zn^{2+}$+$Ni^{2+}$-loaded CS were coated with graphite and then observed under a scanning electron microscope (SEM, JEOL, JSM-6300, Jeol Ltd., Tokyo, Japan) operating at 15 kV and equipped with an energy dispersive X-ray (EDX) detection system.

### 2.9. X-ray Fluorescence (XRF) Spectroscopy

The elemental analyses of the native CS, $Zn^{2+}$-loaded CS, $Ni^{2+}$-loaded CS, and $Zn^{2+}$+$Ni^{2+}$-loaded CS were carried out by XRF (Siemens SRS 3000 spectrometer, Siemens AG, Munich, Germany).

### 2.10. Confocal Laser Scanning Microscopy (CLSM)

Micrographs of the native CS, $Zn^{2+}$-loaded CS, and $Ni^{2+}$-loaded CS were obtained using a Zeiss LSM 710 NLO multiphoton laser scanning confocal microscope (Carl Zeiss Meditec AG, Jena, Germany). Measurements were carried out using Zeiss ZEN software,

and a Zeiss EC Plan-Neofluar 10×/0.3 objective lens was used for scanning. The microscope possessed a fluorescence detection range of 417–729 nm.

## 3. Results and Discussion

### 3.1. Characterization of CS

The specific surface area, total pore volume, and pore diameter are important properties of biosorbents, considered to be indicative of biosorbent effectiveness. The CS average specific surface area, total pore volume, and average pore diameter were found to be 15 $m^2/g$, 0.0326 $cm^3/g$, and 3.209 nm, respectively. The average pore diameter of CS (3.209 nm) indicates that it is a mesoporous biomaterial.

### 3.2. Effect of the Metal Solution pH on the Single and Binary Biosorption of $Zn^{2+}$ and $Ni^{2+}$ Ions

The solution pH is among the foremost operational factors that affects the biosorption of heavy metal ions from aqueous solutions due to the fact that it affects the biosorbent surface charge, the water solubility, and the degree of ionization and speciation of the heavy metal ions. Consequently, the solution pH alters the availability of metal biosorption sites on the biosorbent surface, in addition to influencing competition between the heavy metals present in solution for the biosorption sites [1,39].

Thus, to assess the effects of the solution pH and to determine the optimum pH values for the individual and simultaneous biosorption of $Zn^{2+}$ and $Ni^{2+}$ ions onto CS, equilibrium biosorption trials were performed using metal solutions with pH values ranging from 1.0 to 6.0 (see Figure 1). It is evident from the plots shown in Figure 1 that for both simple and binary metal systems, the biosorption of both $Zn^{2+}$ and $Ni^{2+}$ was negligible between pH 1.0 and 3.0. In contrast, at solution pH values > 3.0, the equilibrium biosorption capacities of both metal ions increased upon increasing the solution pH, thereby confirming that the biosorption of $Zn^{2+}$ and $Ni^{2+}$ ions onto CS is strongly dependent on the solution pH. It was therefore considered that the extremely low levels of biosorption exhibited by CS at lower pH values were due to high electrostatic repulsion between the positively charged metal ions and the positively charged biosorption sites, as well as competition between the metal ions and the high concentration of $H_3O^+$ (which is present at low pH values) for the occupancy of the same biosorption sites. In contrast, at higher solution pH values, the increased $Zn^{2+}$ and $Ni^{2+}$ biosorption levels were attributed to the increasingly anionic character of the CS surface, which resulted in strong electrostatic attractions between the positively charged metals ions and the negatively charged CS surface. Moreover, a lower concentration of $H_3O^+$ would be present at higher pH values, and so the competition between this species and the metal ions for the biosorption sites would also be reduced.

For the monometallic and bimetallic systems, the highest equilibrium biosorption capacities of $Zn^{2+}$ were obtained at solution pH values of 5.0 and 6.0, while the highest equilibrium $Ni^{2+}$ biosorption capacity was attained at a solution pH of 6.0 in the single metal system and at solution pH values of 5.0 and 6.0 in the binary metal system ($p < 0.05$). These results indicate that a pH of 6.0 is optimal for both the individual and simultaneous biosorption of $Zn^{2+}$ and $Ni^{2+}$ ions onto CS biomass, and consequently, this solution pH value was used for all subsequent biosorption experiments. Indeed, previous studies have also reported an optimal solution pH of 6.0 for $Zn^{2+}$ and $Ni^{2+}$ biosorption in monometallic systems [40–42]. Furthermore, Morales-Barrera et al. [1] reported an optimal solution pH of 6.0 for the simultaneous biosorption of $Zn^{2+}$ and $Ni^{2+}$ onto *Lemna gibba* from binary metal solutions.

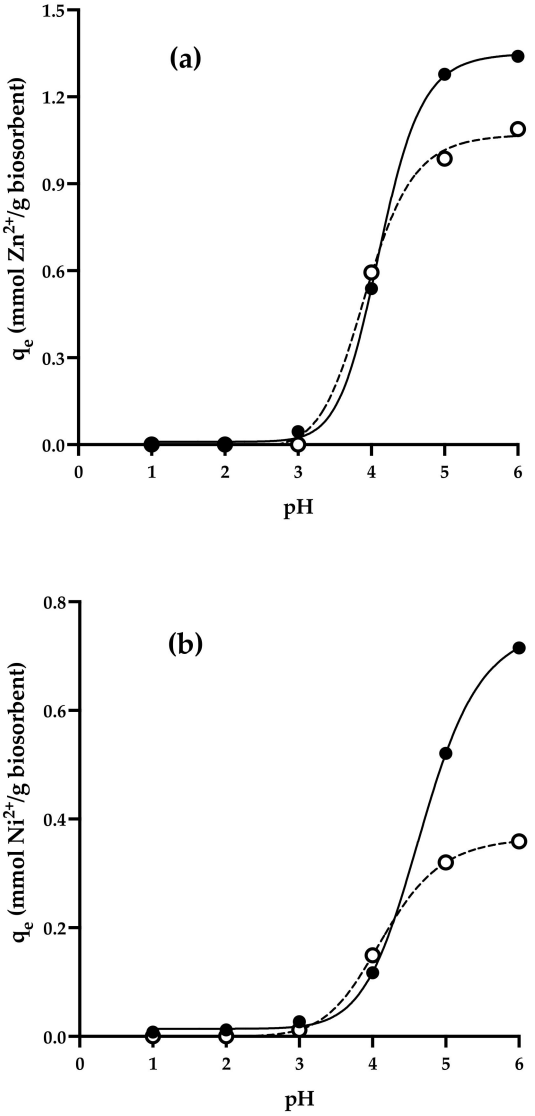


**Figure 1.** Effect of solution pH on the biosorption of (**a**) $Zn^{2+}$ and (**b**) $Ni^{2+}$ ions by CS in single (●) and binary (○) metal systems. Conditions: Biosorbent concentration, 1 g/L; temperature, 25 °C; initial metal concentration, 2 mM. The error bars represent the standard deviation from the mean, and it should be noted that the majority of error bars were smaller than the symbols, and so could not be visualized.

Furthermore, we found that at solution pH values > 3.0, the equilibrium biosorption capacities of $Zn^{2+}$ were greater than those of $Ni^{2+}$ for both the monometallic and the bimetallic systems. Likewise, at solution pH values > 4.0, the biosorption capacities of $Zn^{2+}$ (Figure 1a) and $Ni^{2+}$ (Figure 1b) in the monometallic systems were higher than those of the bimetallic systems, indicating that the biosorptive removal of one heavy metal was adversely affected by the presence of another heavy metal in the bimetallic solution. These results also indicate that $Zn^{2+}$ ions interfered more strongly with $Ni^{2+}$ biosorption onto CS (~50%) than vice versa (~21%), and that the affinity of CS for $Ni^{2+}$ ions is substantially less than for $Zn^{2+}$ ions.

### *3.3. Metal Biosorption Isotherms*

#### 3.3.1. Monometallic Systems

Equilibrium biosorption isotherms and their mathematical modeling are important tools that provide meaningful information on the adsorbate–biosorbent interactions and

the biosorption mechanism, and so are required for the design and optimization of large-scale biosorption processes [43,44]. Thus, Figure 2 displays the experimental isotherms for the biosorption of $Zn^{2+}$ (Figure 2a) and $Ni^{2+}$ (Figure 2b) from monometallic systems onto CS at a solution pH of 6.0 and at 25 ± 1 °C. As indicated, the equilibrium metal biosorption capacities increased with increasing equilibrium concentrations of $Zn^{2+}$ and $Ni^{2+}$ in the aqueous solutions, and this was attributed to the initial metal concentration, which ultimately resulted in enhanced interactions with the CS biosorbent by increasing the probability of interactions between the heavy metal ions and the biosorbent binding sites. Additionally, a higher initial metal concentration leads to a higher metal concentration gradient, which is the thermodynamic driving force that overcomes the mass transfer resistance of the system to increase the equilibrium biosorption capacity [43,45].

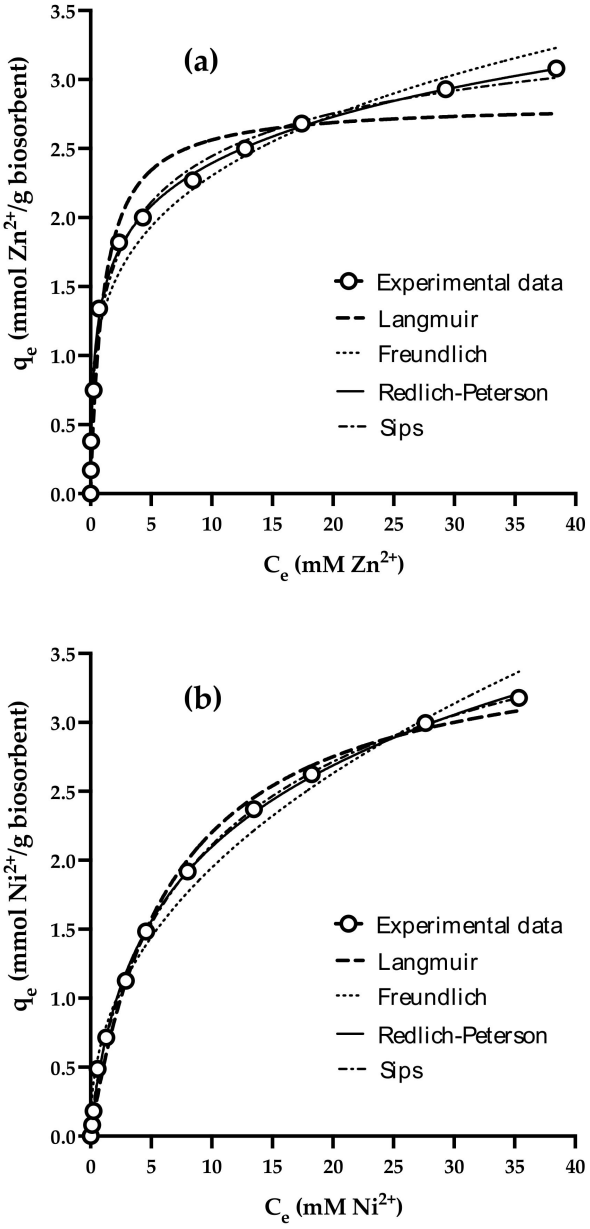


**Figure 2.** Single-component isotherms of (**a**) $Zn^{2+}$ and (**b**) $Ni^{2+}$ on CS and comparison of the different isotherm models in terms of describing the heavy metal biosorption process. Conditions: Biosorbent concentration = 1 g/L; temperature = 25 °C; solution pH = 6.0.

As shown in Figure 2, the $Zn^{2+}$ and $Ni^{2+}$ biosorption isotherms are concave to the concentration axis (i.e., the *x*-axis), which indicates that, as the binding sites for the biosorption of $Zn^{2+}$ and $Ni^{2+}$ ions become occupied, it becomes increasingly more difficult for the remaining heavy metal ions to find vacant binding sites on the CS surface [46] due to the biosorbent surface becoming progressively saturated with metal ions [47]. Likewise, the initial slope and the concave shape of the $Zn^{2+}$ and $Ni^{2+}$ biosorption isotherms show a resemblance with the type L isotherm of the Giles' classification of adsorption isotherms from solute solutions [46]. This isotherm type is generally associated with a high affinity of the biosorbent for the adsorbate, in addition to a minimum competence between the adsorbate and the solvent to occupy the biosorbent binding sites [46,47]. It is noteworthy, however, that the $Zn^{2+}$ and $Ni^{2+}$ biosorption isotherms do not present a plateau, which suggests that the biosorption binding sites of CS are not saturated in the heavy metal concentration range examined herein (i.e., 0–40 mM). We also observed that the $Zn^{2+}$ biosorption isotherm (Figure 2a) shows a higher initial slope than that of the $Ni^{2+}$ biosorption isotherm (Figure 2b), which suggests that CS has a higher preference for $Zn^{2+}$ ions compared to $Ni^{2+}$.

The $Zn^{2+}$ and $Ni^{2+}$ biosorption isotherms were also modeled mathematically using two-parameter (Freundlich and Langmuir) and three-parameter (Sips and Redlich–Peterson) isotherm models to determine the most satisfactory models for describing the equilibrium biosorption processes. Thus, Table 3 shows the parameters of the Freundlich, Langmuir, Redlich–Peterson, and Sips isotherm models for the single metal biosorption of $Zn^{2+}$ and $Ni^{2+}$ ions onto CS, along with their $R^2$, *SSE*, and *RMSE* values. In addition, comparisons between the experimental and predicted equilibrium data are shown in Figure 2.

**Table 3.** Parameters of the mono-component isotherm models for $Zn^{2+}$ and $Ni^{2+}$ biosorption onto CS.

| | | Langmuir | | | |
|---|---|---|---|---|---|
| | $q_m$ | $b_L$ | $R^2$ | *SSE* | *RMSE* |
| $Zn^{2+}$ | 2.827 ± 0.123 | 0.969 ± 0.244 | 0.963 | 0.489 | 0.211 |
| $Ni^{2+}$ | 3.664 ± 0.116 | 0.151 ± 0.014 | 0.994 | 0.085 | 0.088 |
| | | Freundlich | | | |
| | $k_F$ | $n_F$ | $R^2$ | *SSE* | *RMSE* |
| $Zn^{2+}$ | 1.291 ± 0.072 | 3.979 ± 0.308 | 0.978 | 0.292 | 0.163 |
| $Ni^{2+}$ | 0.717 ± 0.055 | 2.304 ± 0.136 | 0.984 | 0.197 | 0.134 |
| | | Redlich–Peterson | | | |
| | $k_{RP}$ | $a_{RP}$ | $b_{RP}$ | $R^2$ | *SSE* | *RMSE* |
| $Zn^{2+}$ | 10.82 ± 2.11 | 6.619 ± 1.485 | 0.824 ± 0.012 | 0.998 | 0.031 | 0.053 |
| $Ni^{2+}$ | 0.977 ± 0.108 | 0.611 ± 0.124 | 0.778 ± 0.026 | 0.999 | 0.014 | 0.035 |
| | | Sips | | | |
| | $q_m$ | $b_S$ | $n_S$ | $R^2$ | *SSE* | *RMSE* |
| $Zn^{2+}$ | 4.011 ± 0.369 | 0.505 ± 0.080 | 0.491 ± 0.048 | 0.995 | 0.062 | 0.075 |
| $Ni^{2+}$ | 4.706 ± 0.242 | 0.147 ± 0.007 | 0.744 ± 0.030 | 0.999 | 0.011 | 0.032 |

As indicated by these data, the highest values for the determination coefficient ($R^2$) and the lowest values for the error functions (*SSE* and *RMSE*) were provided by the Redlich–Peterson and Sips models, and consequently, these isotherm models were considered to be the most suitable for representing the experimental $Zn^{2+}$ and $Ni^{2+}$ biosorption isotherms in monometallic systems. It should be noted here that both the Sips and Redlich–Peterson models are hybrid models that combine the features of the Langmuir and Freundlich isotherms [48,49]. Furthermore, it was found that the Redlich–Peterson ($b_{RP}$) and Sips ($n_s$) isotherm constants deviated from unity, which indicates that the CS surface is heterogeneous in nature [50]. Moreover, the Langmuir isotherm model predicted $b_L$ values between 0 and 1, while the Freundlich isotherm model predicted $n_F$ values between 1 and 10, which both indicate that the biosorptive removal of $Zn^{2+}$ and $Ni^{2+}$ ions by CS was favorable under

the studied conditions [43,51]. Additionally, the $b_L$ and $n_F$ values for $Zn^{2+}$ biosorption were greater than those for the biosorption of $Ni^{2+}$, which again suggests that CS has a higher preference for $Zn^{2+}$ [1].

### 3.3.2. Bimetallic Systems

Figure 3 shows the $Zn^{2+}$ biosorption isotherms in the absence of $Ni^{2+}$ and upon increasing the $Ni^{2+}$ concentration (Figure 3a), in addition to the $Ni^{2+}$ biosorption isotherms at various concentrations of $Zn^{2+}$ ions (Figure 3b).

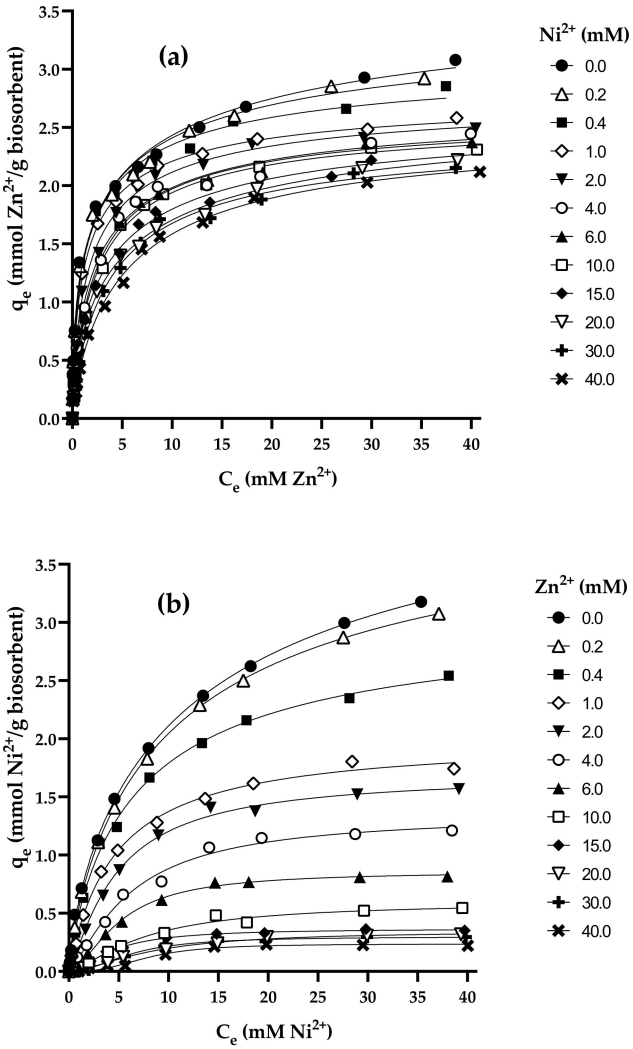


**Figure 3.** (**a**) Biosorption isotherms of $Zn^{2+}$ in the presence of increasing $Ni^{2+}$ concentrations; (**b**) biosorption isotherms of $Ni^{2+}$ in the presence of increasing $Zn^{2+}$ concentrations. Conditions: CS concentration = 1 g/L; temperature = 25 °C; solution pH = 6.0. —: The modified Sips isotherm model prediction.

The results presented in Figure 3 show that the maximum equilibrium biosorption capacity of $Zn^{2+}$ decreased from 3.08 to 2.12 mmol/g upon increasing the initial $Ni^{2+}$ concentration from 0 to 40 mM, which corresponds to a $\leq$31.27% decrease in the equilibrium $Zn^{2+}$ biosorption capacity. Similarly, upon increasing the initial concentration of $Zn^{2+}$ ions from 0 to 40 mM, the maximum equilibrium biosorption capacity of $Ni^{2+}$ ions decreased from 3.18 to 0.221 mmol/g, which represents a $\leq$93% decrease in the presence of $Zn^{2+}$ ions. These results clearly indicate that the biosorption of $Ni^{2+}$ by CS was more adversely

affected by the presence of $Zn^{2+}$ ions than vice versa, further confirming the greater affinity of CS toward $Zn^{2+}$ ions.

The biosorption equilibrium data for $Zn^{2+}$ in the presence of $Ni^{2+}$ ions and those of $Ni^{2+}$ in the presence of $Zn^{2+}$ ions were also represented in the form of three-dimensional (3D) biosorption surfaces (Figure 4). These 3D surface plots confirmed that the biosorption of a single heavy metal is affected, to some degree, by the presence of a second heavy metal in solution, and again indicates that the adverse effect of $Ni^{2+}$ on the biosorption of $Zn^{2+}$ was not as pronounced as the effect of $Zn^{2+}$ ions on the biosorption of $Ni^{2+}$.

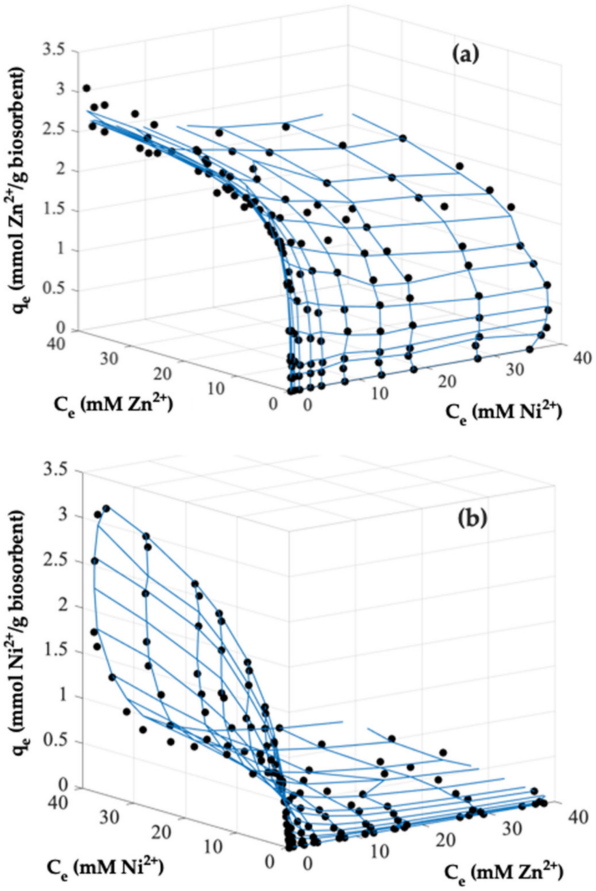


**Figure 4.** Binary biosorption isotherms of $Zn^{2+}$ and $Ni^{2+}$ on CS. (**a**) The effect of $Ni^{2+}$ on the equilibrium biosorption of $Zn^{2+}$ and (**b**) the effect of $Zn^{2+}$ on the equilibrium biosorption of $Ni^{2+}$. The 3D surfaces represent predictions from the modified Sips model, while the black circles represent the experimental data.

In solution, different heavy metals tend to exhibit one of three different types of biosorption behavior: (1) Antagonism, where the effect of mixing the heavy metals is less than the effect achieved for each individual heavy metal; (2) synergism, where the effect of mixing the heavy metals is higher than the effect achieved for each individual heavy metal; and (3) noninteraction, wherein the mixing of heavy metals has no influence on the biosorption of the individual heavy metals present in the mixture (i.e., the effect is the same) [37].

Based on these results, it is apparent that an antagonistic interaction exists between the $Zn^{2+}$ and $Ni^{2+}$ ions during the biosorption process, and this was likely due to competition between the heavy metals for the same biosorption binding sites on the CS surface. The above results also indicate that the affinity of CS for $Zn^{2+}$ ions is greater than that for $Ni^{2+}$ ions, and this may be attributed to the higher atomic weight (65.38 g/mol) and ionic radius (74 pm) of $Zn^{2+}$ compared to the corresponding values for $Ni^{2+}$ (i.e., 58.70 g/mol

and 69 pm, respectively). It has been argued that the higher the atomic weight and ionic radius of a heavy metal, the greater the probability that the heavy metal will interact with the biosorbent binding sites, and the greater the affinity of the biosorbent toward that particular heavy metal [1,52,53]. Based on this assumption, the competitive effects of $Zn^{2+}$ and $Ni^{2+}$ ions are primarily determined by the physicochemical properties of the heavy metals. However, it should be noted that, in a general case, the biosorption capacity is not only related to the properties of the heavy metals, but also the type of biomass employed [54]. Previous studies have shown that the green microalgae *Chlorella kessleri* [55] and the macrophyta *Lemna gibba* [1] also have a greater preference for the biosorption of $Zn^{2+}$ over $Ni^{2+}$.

The above results clearly indicate that the competitive effect is a key factor influencing heavy metal biosorption, and additionally, they highlight the importance of investigating the biosorption capacities of biosorbents in the presence of coexisting heavy metals.

The model bimetallic isotherm parameters were then obtained for the simultaneous biosorption of $Zn^{2+}$ and $Ni^{2+}$ ions by CS, and are listed in Table 4 along with their corresponding error functions. More specifically, the binary biosorption of $Zn^{2+}$ and $Ni^{2+}$ onto CS was best described by the modified Sips isotherm model, which gave the highest $R^2$ and the lowest *SSE* and *RMSE* values. The goodness-of-fit between the experimental data and the data predicted by the modified Sips isotherm model is shown in Figures 3 and 4. The maximum capacities for $Zn^{2+}$ and $Ni^{2+}$ biosorption predicted by the modified Sips isotherm model for the binary metal system were 3.07 and 3.37 mmol/g, respectively (Table 4). CS shows much higher biosorption capacities for $Zn^{2+}$ and $Ni^{2+}$ than those shown by wheat straw [4] and *Lemna gibba* [1].

**Table 4.** Parameters of the binary isotherm models for $Zn^{2+}$ and $Ni^{2+}$ biosorption onto CS.

| | | | | | | | | |
|---|---|---|---|---|---|---|---|---|
| Nonmodified Competitive Langmuir Isotherm | | | | | | | | |
| | $q_{m\ Zn}{}'$ | $q_{m\ Ni}{}'$ | $b_{L\ Zn}{}'$ | | $b_{L\ Ni}{}'$ | $R^2$ | *SSE* | *RMSE* |
| $Zn^{2+}$ | 2.522 ± 0.03 | | 1.132 ± 0.095 | | 0.176 ± 0.021 | 0.969 | 3.580 | 0.159 |
| $Ni^{2+}$ | | 3.255 ± 0.084 | 3.108 ± 0.273 | | 0.21 ± 0.019 | 0.972 | 2.469 | 0.132 |
| Uncompetitive Langmuir isotherm | | | | | | | | |
| | $q_{m\ Zn}{}^*$ | $q_{m\ Ni}{}^*$ | $b_{L\ Zn}{}^*$ | $b_{L\ Ni}{}^*$ | $b^*$ | $R^2$ | *SSE* | *RMSE* |
| $Zn^{2+}$ | 2.54 ± 0.03 | | 1.565 ± 0.16 | 0.919 ± 0.21 | 0.153 ± 0.05 | 0.976 | 2.772 | 0.141 |
| $Ni^{2+}$ | | 3.288 ± 0.09 | 3.396 ± 0.34 | 0.209 ± 0.02 | 0.003 ± 0.002 | 0.972 | 2.414 | 0.131 |
| Partial competitive Langmuir isotherm | | | | | | | | |
| | $q_{max}Zn''$ | $q_{max}Ni''$ | $b_{L\ Zn''}$ | $b_{L\ Ni''}$ | $b_{NiZn}$ | $b_{ZnNi}$ | $R^2$ | *SSE* | *RMSE* |
| $Zn^{2+}$ | 2.73 ± 0.04 | | 1.20 ± 0.1 | 0.89 ± 0.18 | 0.24 ± 0.02 | 0.044 ± 0.01 | 0.972 | 2.069 | 0.122 |
| $Ni^{2+}$ | | 3.69 ± 0.08 | 0.97 ± 0.13 | 0.15 ± 0.01 | 0.67 ± 0.06 | 0.006 ± 0.001 | 0.979 | 2.975 | 0.84 |
| Extended Freundlich isotherm | | | | | | | | |
| | $x_{Zn}$ | $y_{Zn}$ | $z_{Zn}$ | $x_{Ni}$ | $y_{Ni}$ | $z_{Ni}$ | $R^2$ | *SSE* | *RMSE* |
| $Zn^{2+}$ | 0.25 ± 0.03 | 0.23 ± 0.03 | 0.43 ± 0.04 | | | | 0.964 | 4.179 | 0.173 |
| $Ni^{2+}$ | | | | 0.06 ± 0.04 | 0.88 ± 0.11 | 0.85 ± 0.03 | 0.977 | 2.001 | 0.120 |
| Modified Redlich–Peterson isotherm | | | | | | | | |
| | | $\eta_{Zn}$ | | | $\eta_{Ni}$ | | $R^2$ | *SSE* | *RMSE* |
| $Zn^{2+}$ | | 1.678 ± 0.089 | | | 0.865 ± 0.142 | | 0.966 | 3.940 | 0.167 |
| $Ni^{2+}$ | | 1.097 ± 0.110 | | | 0.925 ± 0.046 | | 0.965 | 3.046 | 0.146 |
| Modified Sips isotherm | | | | | | | | |
| | $q_{ms\ Zn}{}'$ | $b_{S\ Zn}{}'$ | $n_{S\ Zn}{}'$ | $q_{ms\ Ni}{}'$ | $b_{S\ Ni}{}'$ | $n_{S\ Ni}{}'$ | $R^2$ | *SSE* | *RMSE* |
| $Zn^{2+}$ | 3.07 ± 0.06 | 0.96 ± 0.07 | 0.64 ± 0.02 | | 0.65 ± 0.09 | 0.45 ± 0.03 | 0.992 | 0.986 | 0.084 |
| $Ni^{2+}$ | | 1.54 ± 0.17 | 0.85 ± 0.03 | 3.37 ± 0.54 | 0.15 ± 0.02 | 0.65 ± 0.03 | 0.984 | 1.391 | 0.100 |

### *3.4. DRIFTS Studies*

The DRIFTS spectra of the native CS and the CS loaded with $Zn^{2+}$, $Ni^{2+}$, and $Zn^{2+}$+$Ni^{2+}$ ions were then compared to identify the binding sites that may be involved in the biosorption of the heavy metals (Figure 5), while the main infrared absorption bands observed in the DRIFTS spectra are listed in Table 5.

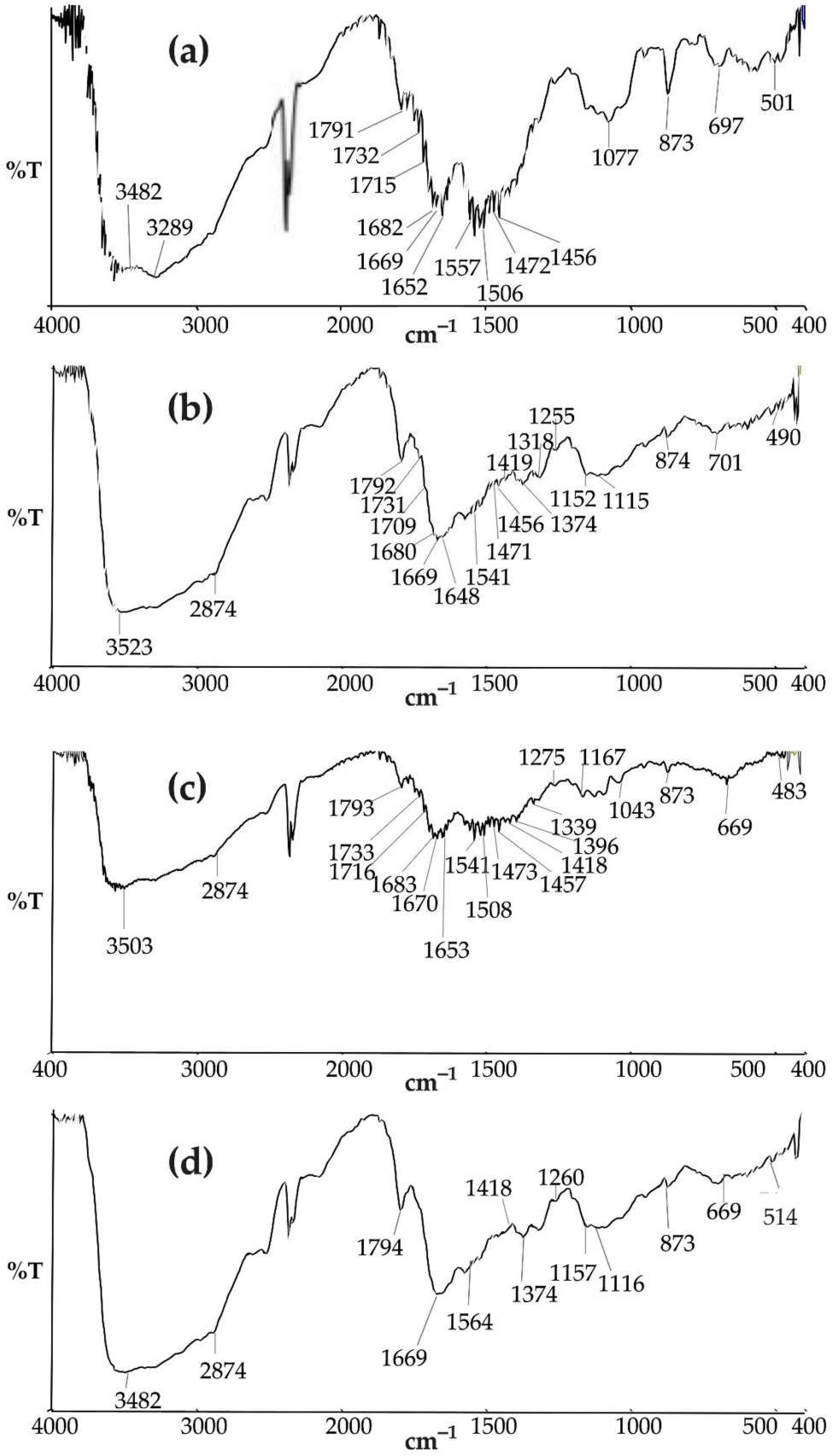


**Figure 5.** DRIFTS spectra of (**a**) the native CS and the CS loaded with (**b**) $Zn^{2+}$, (**c**) $Ni^{2+}$, and (**d**) $Zn^{2+}$+$Ni^{2+}$ ions.

It has previously been reported that *Callinectes sapidus* crab shell is composed of ~30–50 *w/w*% $CaCO_3$ [56], 25 *w/w*% proteins [57], ≤30 *w/w*% chitin [56], and a low content of lipids [58,59]. Based on these reports and the obtained DRIFTS spectrum for the native CS, several absorption bands were identified relating to these components, including the C=O stretching vibration of $CO_3^{2-}$ at 1791 $cm^{-1}$ [60], the C–O stretching vibration of the ring COH and of the COC and $CH_2OH$ groups of chitin at 1077 $cm^{-1}$ [61], the C=O stretching vibrations of the chitin and protein amide I bands at 1680–1650 $cm^{-1}$ [62], the C-N stretching and N-H bending vibrations of the chitin and protein amide II bands at 1560–1530 $cm^{-1}$ [62], and the C=O stretching vibration of the fatty acid carboxylic and/or ester groups at 1732 $cm^{-1}$ [63].

**Table 5.** Main vibration frequencies found in the DRIFTS spectra of the native CS and the CS loaded with $Zn^{2+}$, $Ni^{2+}$, and $Zn^{2+}$+$Ni^{2+}$ ions.

| Referenced Frequency ($cm^{-1}$) | Functional Groups Involved | Native CS | $Zn^{2+}$-Loaded CS | $Ni^{2+}$-Loaded CS | $Zn^{2+}$+$Ni^{2+}$-Loaded CS | Reference |
|---|---|---|---|---|---|---|
| | | Frequency in This Work ($cm^{-1}$) | | | | |
| 3600–2600 | OH, CH and NH stretching vibration | 3600–2600 | 3600–2600 | 3600–2600 | 3600–2600 | [62] |
| 2877 | CH stretching in chitin ring | ND | 2874 | 2874 | 2874 | [61] |
| 1800 | C=O stretching vibration of $CO_3^{2-}$ | 1791 | 1792 | 1793 | 1794 | [60] |
| 1740 | C=O stretching vibration of carboxylic or ester group of fatty acids | 1732 | 1731 | 1733 | ND | [63] |
| 1680–1650 | C=O stretching of amide I of chitin and proteins | 1669 | 1669 | 1670 | 1669 | [62] |
| 1560–1530 | N–H bending and C–N stretching of amide II of chitin and proteins | 1557 | 1541 | 1541 | 1564 | [62] |
| 1383 | CH deformation in amide II | ND | 1374 | 1396 | ND | [64] |
| 1320 | C-N stretching vibration of amide III | ND | 1318 | 1339 | ND | [65] |
| 1260 | C-O stretching of COOH | ND | 1255 | 1275 | 1260 | [52,65] |
| 1074 | Stretching vibrations of C–O on the structure of the chitin ring | 1077 | 1115 | 1043 | 1116 | [61] |

ND = Not detected.

The absorption spectra of the CS loaded with $Zn^{2+}$, $Ni^{2+}$ and $Zn^{2+}$+$Ni^{2+}$ ions showed several changes with respect to that of the native biosorbent, such as the appearance of new absorption bands, increases in the band amplitudes and intensities, and shifts in the band positions. These changes were suggestive of interactions between the heavy metals and the functional groups present on the CS surface. For example, one important change involved the absorption band corresponding to the C=O stretching vibration of $CO_3^{2-}$, which was better defined in the spectra of the heavy metal-loaded biosorbent, which suggests that $CaCO_3$ is involved in the removal of $Zn^{2+}$ and $Ni^{2+}$ from both monometallic and bimetallic solutions by CS. Indeed, previous studies have reported that $CaCO_3$ plays a significant role in the adsorption of several heavy metals from aqueous solutions, such as lead, cadmium, copper, and chromium by crab shells [66,67].

Furthermore, a new absorption band appeared at 2874 $cm^{-1}$ in the DRIFS spectra of the CS loaded with $Zn^{2+}$, $Ni^{2+}$, and $Zn^{2+}$+$Ni^{2+}$ ions; this band was attributed to the stretching vibration of the chitin CH bonds, thereby suggesting that some of the $CaCO_3$ present in the crab shell dissolved in the aqueous solution to expose a number of chitin functional groups. It should also be noted here that during our study, before the solution pH reached a stable value of 6.0, an increase in pH was observed when CS particles were added to the single and binary metal solutions of $Zn^{2+}$ and $Ni^{2+}$; this increase was therefore attributed to the dissolution of $CaCO_3$ to produce $CO_3^{2-}$ in solution. In this context, it has been previously proposed that the carbonate ions in solution (i.e., from the dissolved $CaCO_3$ present in the crab shell) can combine with divalent cationic heavy metals to form metal carbonates, which can then be biosorbed to chitin on the crab shell surface [27,66], and so it is possible that this reaction was also taking place in our system.

A change in the infrared band shape corresponding to the C=O stretching vibration (1669 $cm^{-1}$) of the amide I group [62], as well as a change in the amide II (C-N stretching and N-H bending) band width at 1564–1541 $cm^{-1}$ [62], were also observed in the DRIFTS

spectra of the heavy metal-loaded biosorbent, which suggests the interaction of $Zn^{2+}$ and $Ni^{2+}$ with the amide functional groups of CS.

Moreover, new absorption bands appeared in the DRIFTS spectra of the heavy metal-loaded biosorbent at 1383 and 1320 $cm^{-1}$, which were assigned to the amide II C-H deformation vibration [64] and the amide III C-N stretching vibration [65], respectively. These findings strengthen the evidence for the involvement of amide functional groups in the biosorption of $Zn^{2+}$ and $Ni^{2+}$ ions by CS. Another important change was the appearance of an absorption band at 1260 $cm^{-1}$, which was assigned to the C-O stretching vibration of the COOH groups [52].

The above results therefore clearly indicate that the $CO_3^{2-}$ ion, in addition to the amide and carboxylic functional groups present in the chitin and protein components of crab shell, play major roles in the CS biosorption of $Zn^{2+}$ and $Ni^{2+}$ from aqueous solutions.

### *3.5. EDX Analysis*

The EDX spectra of the native, $Zn^{2+}$-loaded, $Ni^{2+}$-loaded, and $Zn^{2+}$+$Ni^{2+}$-loaded CS are shown in Figure 6. As indicated, strong calcium (Ca) peaks can be observed in the spectrum of the native CS (Figure 6a), which confirms the presence of $CaCO_3$ in this biosorbent. Peaks were also observed for carbon (C), oxygen (O), magnesium (Mg), sodium (Na), potassium (K), chlorine (Cl), and phosphorus (P), but no peaks were found for zinc and/or nickel on the surface of native CS. In contrast, strong peaks corresponding to zinc (Figure 6b), nickel (Figure 6c), and zinc + nickel (Figure 6d) were observed on the CS surface after biosorption from the corresponding aqueous solutions, thereby confirming the successful biosorption of these ions onto CS.

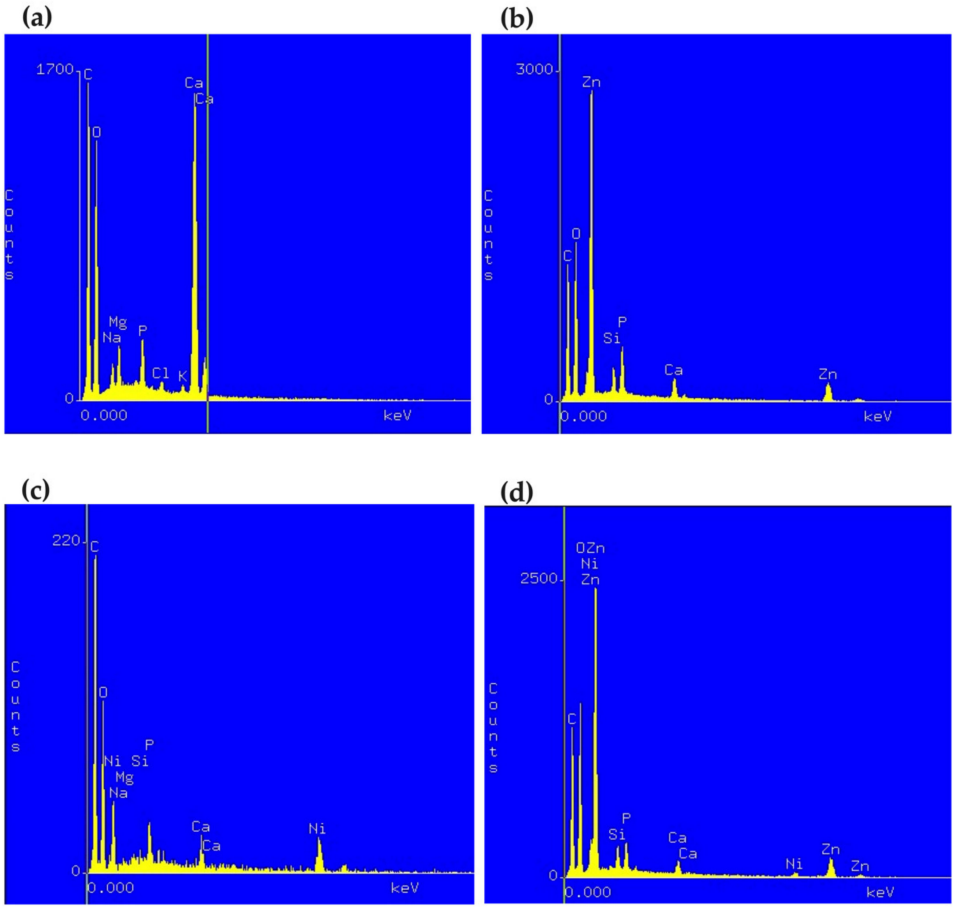


**Figure 6.** EDX spectra of (**a**) the native CS and the CS loaded with (**b**) $Zn^{2+}$, (**c**) $Ni^{2+}$, and (**d**) $Zn^{2+}$+$Ni^{2+}$.

Importantly, in the EDX spectra of the $Zn^{2+}$-loaded, $Ni^{2+}$-loaded, and $Zn^{2+}$+$Ni^{2+}$-loaded CS, the intensity of the calcium peak was significantly reduced compared with that observed in the native CS, which suggests that calcium ions were leached out from the CS, and that nickel and zinc carbonate species were present on the CS surface. Similar findings and conclusions were reported by Vijayaraghavan et al. [27] in their studies on the crab shell biosorption of $Mn^{2+}$ and $Zn^{2+}$ from aqueous solutions.

### *3.6. XRF Analysis*

XRF studies were then conducted to assess the different chemical compositions of the native, $Zn^{2+}$-loaded, $Ni^{2+}$-loaded, and $Zn^{2+}$+$Ni^{2+}$-loaded CS, and results are listed in Table 6.

**Table 6.** XRF analyses of the native, $Zn^{2+}$-loaded, $Ni^{2+}$-loaded, and $Zn^{2+}$+$Ni^{2+}$-loaded CS.

| | % | | | |
|---|---|---|---|---|
| **Component** | **Native CS** | **$Zn^{2+}$-Loaded CS** | **$Ni^{2+}$-Loaded CS** | **$Zn^{2+}$+$Ni^{2+}$-Loaded CS** |
| ZnO | 0.03 | 43.9 | 0.03 | 44.00 |
| NiO | 0.01 | 0.02 | 52.1 | 8.29 |
| CaO | 32.68 | 16.51 | 13.83 | 13.73 |
| Trace metals | 9.05 | 10.07 | 9.44 | 9.45 |
| LOI | 58.23 | 29.5 | 24.6 | 24.53 |

It is evident that the most abundant component of the native CS is calcium (i.e., CaO, 32.68%), which is present in the form of calcium carbonate in crab shells [56,68]. In addition, CS contains 9.05% trace elements, which mainly include phosphorus, magnesium, sodium, aluminum, and potassium. As indicated by the XRF results, its zinc and nickel contents are negligible. Furthermore, CS was found to contain an organic content of 58.23%, which was attributed to the chitin and protein components, and was determined based on the loss of ignition (LOI).

In contrast, following the biosorption of $Zn^{2+}$ and $Ni^{2+}$ from single metal systems, the zinc and nickel contents of the heavy metal-loaded CS increased to 43.9% (ZnO) and 52.1% (NiO), respectively. Similarly, for the binary metal system, the zinc and nickel contents in the $Zn^{2+}$+$Ni^{2+}$-loaded CS were determined to be 44% (ZnO) and 8.29% (NiO), respectively; this higher zinc content further confirms the greater affinity of CS toward $Zn^{2+}$, as discussed above. Overall, these results clearly confirm the biosorption of $Zn^{2+}$ and $Ni^{2+}$ onto CS, both from single and the binary metal solution systems.

Notably, the calcium content (CaO) of $Zn^{2+}$-loaded, $Ni^{2+}$-loaded, and $Zn^{2+}$+$Ni^{2+}$-loaded CS was approximately half that of the native CS, which can be attributed to the dissolution of some of the $CaCO_3$ present in CS after coming into contact with $Zn^{2+}$ and/or $Ni^{2+}$ solutions. These findings corroborate the results obtained in the FTIR and SEM-EDX studies. Contrastingly, the trace element content of $Zn^{2+}$-loaded, $Ni^{2+}$-loaded, and $Zn^{2+}$+$Ni^{2+}$-loaded CS was similar to that of native CS, possibly due to the fact that these elements were not exchanged during the biosorption processes.

### *3.7. CLSM Studies*

One of the advantages of CLSM is its ability to display autofluorescent components present in a sample that exhibit different emission wavelengths in different colors, without the need for staining. Thus, in the present work, this technique was used to demonstrate the presence of heavy metals on the surface of CS loaded with $Zn^{2+}$ and $Ni^{2+}$. Figures 7a, 8a and 9a display the optical micrographs recorded at a magnification of 20× for the native, $Zn^{2+}$-loaded, and $Ni^{2+}$-loaded CS, respectively. Likewise, Figure 7b–d, Figures 8b–e and 9b–e correspond to the confocal micrographs of the above three CS systems, respectively. As indicated, the native CS exhibits two maximum emission wavelengths ($E_m$) in its emission spectrum, namely at 519 nm (in red, Figure 7b) and 461 nm (in blue, Figure 7c). To verify that this fluorescence originated from the biosorbent

sample, the optical (Figure 7a) and confocal (Figure 7b–d) micrographs of the native CS were overlapped to generate the overlay image shown in Figure 7d.

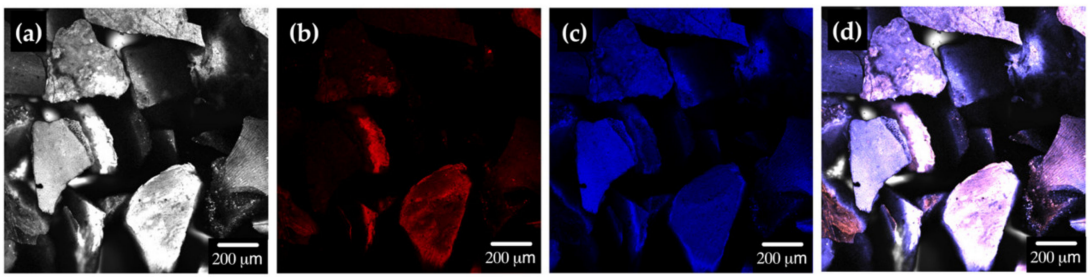


**Figure 7.** Optical (**a**) and confocal micrographs of native CS at 519 nm (**b**) and 461 nm (**c**). Overlay image of native CS (**d**).

In addition, as shown in Figures 8d and 9d, both $Zn^{2+}$ and $Ni^{2+}$ exhibited autofluorescence at an $E_m$ of 636 nm (in green), and consequently, the CLSM assays could only be performed using the samples loaded with a single heavy metal and not with both metals. Thus, Figure 8b–d show the confocal micrographs of CS loaded with $Zn^{2+}$ at emission wavelengths of 519, 461, and 636 nm, respectively, while Figure 9b–d show the corresponding images for $Ni^{2+}$ loading. The overlay images of the CS specimens loaded with $Zn^{2+}$ and $Ni^{2+}$ are shown in Figures 8e and 9e, wherein it can be clearly observed that these metal ions were present on the CS surface.

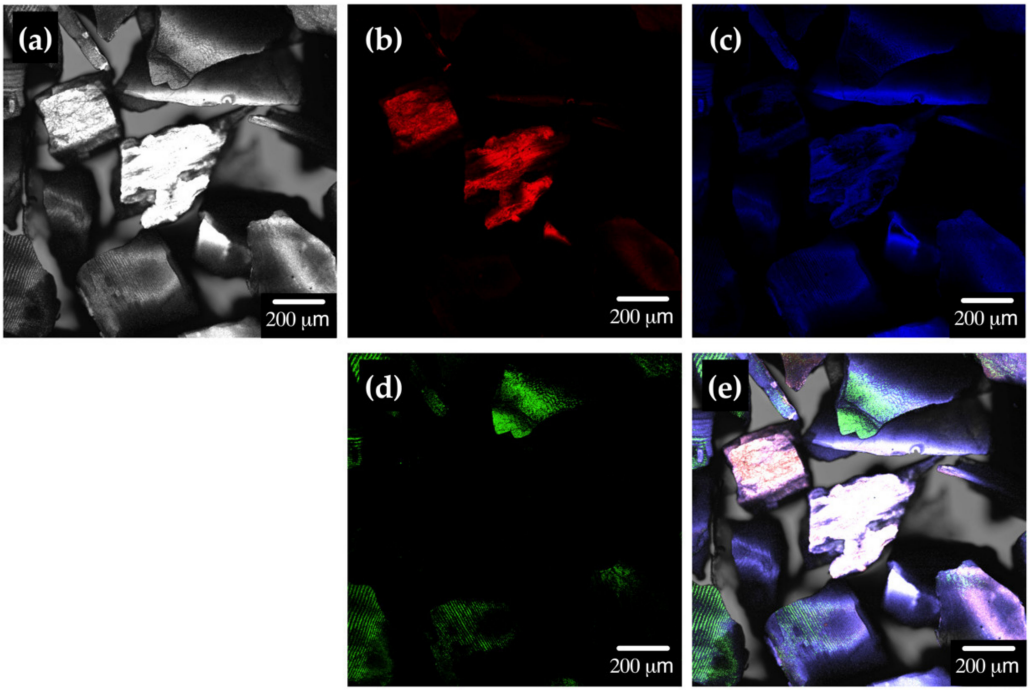


**Figure 8.** (**a**) Optical and (**b**–**d**) confocal micrographs of the $Zn^{2+}$-loaded CS at (**b**) 519 nm, (**c**) 461 nm, and (**d**) 636 nm. (**e**) Overlay of all four images for the $Zn^{2+}$-loaded CS.

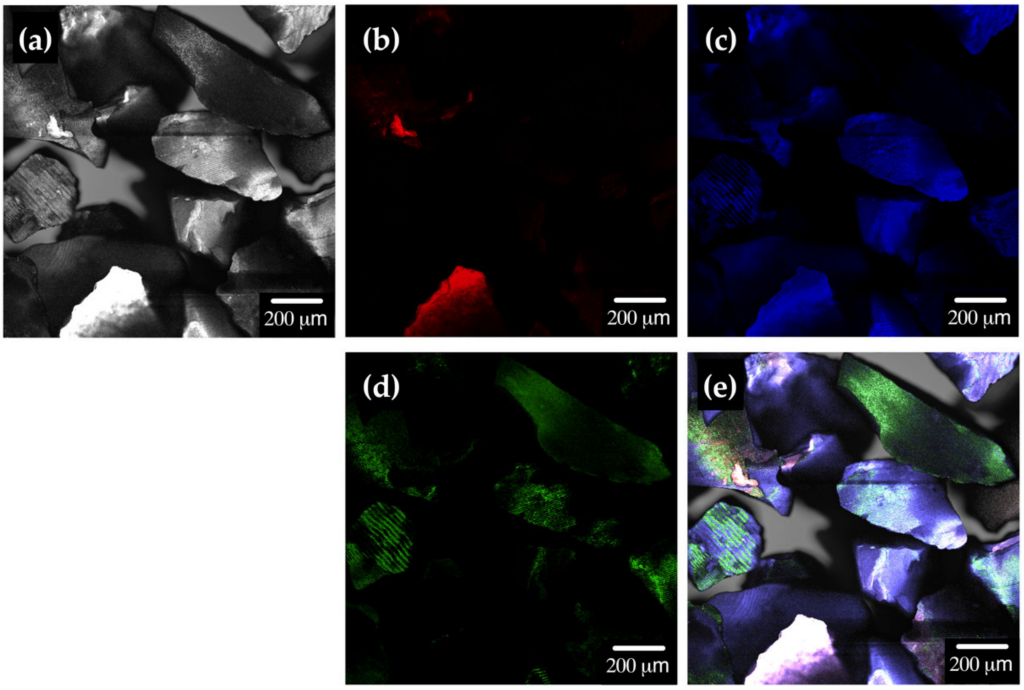


**Figure 9.** (**a**) Optical and (**b**–**d**) confocal micrographs of the $Ni^{2+}$-loaded CS at (**b**) 519 nm, (**c**) 461 nm, and (**d**) 636 nm. (**e**) Overlay of all four images for the $Ni^{2+}$-loaded CS.

## 4. Conclusions

The present work investigated the potential for using crab shell (CS) as a heavy metal biosorbent to individually and simultaneously remove $Zn^{2+}$ and $Ni^{2+}$ from aqueous solutions. Upon examination of the optimal conditions for the biosorption process, it was found that the solution pH had a significant effect in both the monometallic and bimetallic systems, and a pH of 6.0 was determined to be optimal for the individual and simultaneous removal of $Zn^{2+}$ and $Ni^{2+}$ ions. In addition, the single and binary biosorption equilibrium data obtained for the removal of $Zn^{2+}$ and $Ni^{2+}$ by CS indicated that the affinity of CS toward $Zn^{2+}$ was higher than that toward $Ni^{2+}$. Furthermore, the binary biosorption isotherms of $Zn^{2+}$ and $Ni^{2+}$ showed that the equilibrium biosorption capacity of one heavy metal decreased as the initial concentration of the other heavy metal increased, and this was attributed to competition between the two heavy metals for the CS biosorption binding sites. A high antagonistic effect of $Zn^{2+}$ ions on the biosorption of $Ni^{2+}$ was observed, although the biosorption of $Zn^{2+}$ was affected to a considerably lesser extent by the presence of $Ni^{2+}$ ions. The competitive effects between these two heavy metal ions were determined mainly by their physicochemical properties, and our results indicate that this competitive effect is a key factor influencing heavy metal biosorption, thereby highlighting the importance of investigating the biosorption capacities of biosorbents in the presence of coexisting heavy metals. Moreover, the individual biosorption of $Zn^{2+}$ and $Ni^{2+}$ ions from aqueous solutions by CS was best described by the Sips and Redlich–Peterson isotherm models, while the simultaneous biosorption of both heavy metals was best represented by the modified Sips isotherm model. Finally, the results of analysis by diffuse reflectance infrared Fourier transform spectroscopy indicated that the carbonate, carboxyl, and amide functional groups of CS were involved in the biosorption of $Zn^{2+}$ and $Ni^{2+}$ ions, and the biosorption of these ions on the CS surface was confirmed by X-ray fluorescence spectroscopy, scanning electron microscopy coupled with energy dispersive X-ray spectroscopy, and confocal laser scanning microscopy. These results are expected to contribute to the development of more efficient and effective biosorbents for the removal of heavy metal contamination from wastewater systems.

**Author Contributions:** Conceptualization, E.C.-U.; methodology, L.M.-B. and E.C.-U.; software, L.M.-B.; validation, L.M.-B.; formal analysis, L.M.-B. and E.C.-U.; investigation, L.M.-B.; resources, E.C.-U.; writing—original draft preparation, L.M.-B. and E.C.-U.; visualization, L.M.-B.; supervision, E.C.-U.; project administration, E.C.-U.; funding acquisition, E.C.-U. All authors have read and agreed to the published version of the manuscript.

**Funding:** This research was funded by the Instituto Politécnico Nacional (IPN), Secretaría de Investigación y Posgrado, Grant Number: SIP20220923.

**Acknowledgments:** The authors acknowledge the technical support provided by the Centro de Nanociencias y Micro y Nanotecnologías, at the IPN. L.M.-B. and E.C.-U. hold grants from EDI-IPN, COFAA-IPN, and SNI-CONACYT.

**Conflicts of Interest:** The authors declare no conflict of interest.

## References

1. Morales-Barrera, L.; Flores-Ortiz, C.M.; Cristiani-Urbina, E. Single and binary equilibrium studies for $Ni^{2+}$ and $Zn^{2+}$ biosorption onto *Lemna gibba* from aqueous solutions. *Processes* **2020**, *8*, 1089. [CrossRef]
2. King, P.; Anuradha, K.; Beena Lahari, S.B.; Prasanna Kumar, Y.; Prasad, V.S.R.K. Biosorption of zinc from aqueous solution using *Azadirachta indica* bark: Equilibrium and kinetic studies. *J. Hazard. Mater.* **2008**, *152*, 324–329. [CrossRef] [PubMed]
3. Öztürk, A. Removal of nickel from aqueous solution by the bacterium *Bacillus thuringiensis*. *J. Hazard. Mater.* **2007**, *147*, 518–523. [CrossRef]
4. Baig, K.S.; Doan, H.D.; Wu, J. Multicomponent isotherms for biosorption of $Ni^{2+}$ and $Zn^{2+}$. *Desalination* **2009**, *249*, 429–439. [CrossRef]
5. Lu, S.; Gibb, S.W.; Cochrane, E. Effective removal of zinc ions from aqueous solutions using crab carapace biosorbent. *J. Hazard. Mater.* **2007**, *149*, 208–217. [CrossRef] [PubMed]
6. Pandey, P.K.; Choubey, S.; Verma, Y.; Pandey, M.; Kalyan-Kamal, S.S.; Chandrashekhar, K. Biosorptive removal of Ni(II) from wastewater and industrial effluent. *Int. J. Environ. Res. Public Health* **2007**, *4*, 332–339. [CrossRef]
7. Subbaiah, M.V.; Vijaya, Y.; Kumar, N.S.; Redddy, A.S.; Abburi, K. Biosorption of nickel from aqueous solutions by *Acacia leucocephala* bark: Kinetics and equilibrium studies. *Colloids Surf. B Biointerfaces* **2009**, *74*, 260–265. [CrossRef]
8. Savolainen, H. Biochemical and clinical aspects of nickel toxicity. *Environ. Health Rev.* **1996**, *11*, 167–173. [CrossRef]
9. Fosmire, G.J. Zinc toxicity. *Am. J. Clin. Nutr.* **1990**, *51*, 225–227. [CrossRef]
10. Plum, L.M.; Rink, L.; Haase, H. The essential toxin: Impact of zinc on human health. *Int. J. Environ. Res. Public Health* **2010**, *7*, 1342–1365. [CrossRef]
11. World Health Organization (WHO). *Zinc in Drinking Water. Background Document for Development of WHO Guidelines for Drinking-Water Quality*; WHO/SDE/WSH/03.04/17; World Health Organization: Geneva, Switzerland, 2003.
12. World Health Organization (WHO). *Nickel in Drinking Water. Background Document for Development of WHO Guidelines for Drinking-Water Quality*; WHO/SDE/WSH/05.08/55; World Health Organization: Geneva, Switzerland, 2005.
13. Kurniawan, T.A.; Chan, G.Y.Z.; Lo, W.-H.; Babel, S. Physico-chemical treatment techniques for wastewater laden with heavy metals. *Chem. Eng. J.* **2006**, *118*, 83–98. [CrossRef]
14. Zafar, M.N.; Nadeem, R.; Hanif, M.A. Biosorption of nickel from protonated rice bran. *J. Hazard. Mater.* **2007**, *145*, 501–505. [CrossRef] [PubMed]
15. Ramírez-Rodríguez, A.; Reyes-Ledezma, J.L.; Chávez-Camarillo, G.M.; Cristiani-Urbina, E.; Morales-Barrera, L. Cyclic biosorption and desorption of acid red 27 onto *Eichhornia crassipes* leaves. *Rev. Mex. Ing. Quim.* **2018**, *17*, 1121–1134. [CrossRef]
16. Ramírez-Rodríguez, A.; Morales-Barrera, L.; Cristiani-Urbina, E. Continuous biosorption of acid red 27 azo dye by *Eichhornia crassipes* leaves in a packed-bed column. *Sci. Rep.* **2021**, *11*, 18413. [CrossRef] [PubMed]
17. Febrianto, J.; Kosasih, A.N.; Sunarso, J.; Ju, Y.H.; Indraswati, N.; Ismadju, S. Equilibrium and kinetic studies in adsorption of heavy metals using biosorbent: A summary of recent studies. *J. Hazard. Mater.* **2009**, *162*, 616–645. [CrossRef]
18. Mehta, S.K.; Gaur, J.P. Concurrent sorption of $Ni^{2+}$ and $Cu^{2+}$ by *Chlorella vulgaris* from a binary metal solution. *Appl. Microbiol. Biotechnol.* **2001**, *55*, 379–382. [CrossRef]
19. Aksu, Z.; Dönmez, G. Binary biosorption of cadmium(II) and nickel(II) onto dried *Chlorella vulgaris*: Co-ion effect on mono-component isotherm parameters. *J. Hazard. Mater.* **2006**, *41*, 860–868. [CrossRef]
20. Luna, A.S.; Costa, A.L.H.; da Costa, A.C.A.; Henriques, C.A. Competitive biosorption of cadmium(II) and zinc(II) ions from binary systems by *Sargassum filipendula*. *Bioresour. Technol.* **2010**, *101*, 5104–5111. [CrossRef]
21. Oliveira, E.A.; Montanher, S.F.; Andrade, A.D.; Nóbrega, J.A.; Rollemberg, M.C. Equilibrium studies for the sorption of chromium and nickel from aqueous solutions using raw rice bran. *Process Biochem.* **2005**, *40*, 3485–3490. [CrossRef]
22. Monteiro, R.J.R.; Lopes, C.B.; Rocha, L.S.; Coelho, J.P.; Duarte, A.C.; Pereira, E. Sustainable approach for recycling seafoods wastes for the removal of priority hazardous substances (Hg and Cd) from water. *J. Environ. Chem. Eng.* **2016**, *4*, 1199–1208. [CrossRef]
23. Kim, D.S. The removal by crab shell of mixed heavy metal ions in aqueous solution. *Bioresour. Technol.* **2003**, *87*, 355–357. [CrossRef]

24. Vijayaraghavan, K.; Padmesh, T.V.N.; Palanivelu, K.; Velan, M. Biosorption of nickel(II) ions onto *Sargassum wightii:* Application of two-parameter and three-parameter isotherm models. *J. Hazard. Mater.* **2006**, *133*, 304–308. [CrossRef] [PubMed]
25. Niu, H.; Volesky, B. Biosorption of chromate and vanadate species with waste crab shells. *Hydrometallurgy* **2006**, *84*, 28–36.
26. Dahiya, S.; Tripathi, R.M.; Hegde, A.G. Biosorption of lead and copper from aqueous solutions by pre-treated crab and arca shell biomass. *Bioresour. Technol.* **2008**, *99*, 179–187. [CrossRef]
27. Vijayaraghavan, K.; Winnie, H.Y.N.; Balasubramanian, R. Biosorption characteristics of crab shell particles for the removal of manganese(II) and zinc(II) from aqueous solutions. *Desalination* **2011**, *266*, 195–200. [CrossRef]
28. Murugesan, S.; Rajiv, S.; Thanapalan, M. Optimization of process variables for a biosorption of nickel(II) using response surface method. *Korean J. Chem. Eng.* **2009**, *26*, 364–370. [CrossRef]
29. Morales-Barrera, L. Estudio de la Remoción de Metales Pesados de Soluciones Acuosas por Materiales Biológicos. Ph.D. Thesis, Escuela Nacional de Ciencias Biológicas, Instituto Politécnico Nacional, Ciudad de Mexico, Mexico, 2012.
30. Hach Company. *Hach Water Analysis Handbook*; Hach Company: Hach, Loveland, 2008.
31. Gupta, V.K.; Suhas; Nayak, A.; Agarwal, S.; Chaudhary, M.; Tyagi, I. Removal of Ni(II) ions from water using scrap tire. *J. Mol. Liq.* **2014**, *190*, 215–222. [CrossRef]
32. Vaguetti, J.C.P.; Lima, E.C.; Royer, B.; Brasil, J.L.; da Cunha, B.M.; Simon, N.M.; Cardoso, N.F.; Zapata-Noreña, C.P. Application of Brazilian-pine fruit coat as a biosorbent to removal of Cr(VI) from aqueous solution—Kinetics and equilibrium study. *Biochem. Eng. J.* **2008**, *42*, 67–76. [CrossRef]
33. Mohan, D.; Pittman, U., Jr. Activated carbons and low cost adsorbents for remediation of tri- and hexavalent chromium from water. *J. Hazard. Mater.* **2006**, *137*, 762–811. [CrossRef]
34. Aksu, Z.; Balibek, E. Chromium (VI) biosorption by dried *Rhizopus arrhizus*: Effect of salt (NaCl) concentration on equilibrium and kinetic parameters. *J. Hazard. Mater.* **2007**, *145*, 210–220. [CrossRef]
35. Mckay, G.; Porter, J.F. A comparison of Langmuir based models for predicting multicomponent metal ion equilibrium sorption isotherms on peat. *Trans. IChemE* **1997**, *75*, 171–180. [CrossRef]
36. Apiratikul, R.; Pavasant, P. Sorption isotherm model for binary component sorption of copper, cadmium, and lead ions using dried green macroalga, *Caulerpa lentillifera*. *Chem. Eng. J.* **2006**, *119*, 135–145. [CrossRef]
37. Srivastava, V.C.; Mall, I.D.; Mishra, I.M. Equilibrium modelling of single and binary adsorption of cadmium and nickel onto bagasse fly ash. *Chem. Eng. J.* **2006**, *117*, 79–91. [CrossRef]
38. Yesuf, J.N.; DeVantier, B.A.; Chevalier, L.R. Bisolute equilibrium studies for the sorption of basic dyes on a GAC from almond shells: A nonlinear approach. *Water Air Soil Pollut.* **2008**, *8*, 387–393. [CrossRef]
39. Kumar, D.; Pandey, L.K.; Gaur, J.P. Metal sorption by algal biomass: From batch to continuous system. *Algal Res.* **2016**, *18*, 95–109. [CrossRef]
40. Liu, Y.; Fan, T.; Zen, G.-M.; Li, X.; Tong, Q.; Ye, F.; Zhou, M.; Xu, W.-H.; Huang, Y.-E. Removal of cadmium and zinc ions from aqueous solution by living *Aspergillus niger*. *Trans. Nonferrous Met. Soc. China* **2006**, *16*, 681–686. [CrossRef]
41. Salam, O.E.A.; Reiad, N.A.; Elshafei, M.M. A study of the removal characteristics of heavy metals from wastewater by low-cost adsorbents. *J. Adv. Res.* **2011**, *2*, 297–303. [CrossRef]
42. Saygideger, S.; Gülnaz, O.; Istifli, E.S.; Yucel, N. Adsorption of Cd(II), Cu(II), and Ni(II) ions by *Lemna minor* L.: Effect of physicochemical environment. *J. Hazard. Mater.* **2005**, *126*, 96–104. [CrossRef]
43. Aranda-García, E.; Cristiani-Urbina, E. Kinetic, equilibrium, and thermodynamic analyses of Ni(II) biosorption from aqueous solution by acorn shell of *Quercus crassipes*. *Water Air Soil Pollut.* **2018**, *229*, 119. [CrossRef]
44. Yadav, M.; Das, M.; Savani, C.; Thakore, S.; Jadeja, R. Maleic anhydride cross-linked β-cyclodextrin-conjugated magnetic nanoadsorbent: An ecofriendly approach for simultaneous adsorption of hydrophilic and hydrophobic dyes. *ACS Omega* **2019**, *4*, 11993–12003. [CrossRef]
45. Aranda-García, E.; Cristiani-Urbina, E. Hexavalent chromium removal and total chromium biosorption from aqueous solution by *Quercus crassipes* acorn shell in a continuous up-flow fixed-bed column: Influencing parameters, kinetics, and mechanism. *PLoS ONE* **2020**, *15*, e0227953. [CrossRef] [PubMed]
46. Giles, C.H.; MacEwan, T.H.; Nakhwa, S.N.; Smith, D. Studies in adsorption. Part XI. A system of classification of solution adsorption isotherms, and its use in diagnosis of adsorption mechanisms and in measurement of specific surface areas of solids. *J. Chem. Soc.* **1960**, *3*, 3973–3993. [CrossRef]
47. Limousin, G.; Gaudet, J.P.; Charlet, L.; Szenknect, S.; Barthès, V.; Krimissa, M. Sorption isotherms: A review on physical bases, modeling and measurement. *J. Appl. Geochem.* **2007**, *22*, 249–275. [CrossRef]
48. Al-Ghouti, M.A.; Da'ana, D.A. Guidelines for the use and interpretation of adsorption isotherm models: A review. *J. Hazard. Mater.* **2020**, *393*, 122383. [CrossRef]
49. Majd, M.M.; Kordzadeh-Kermani, V.; Ghalandari, V.; Askari, A.; Sillanpää, M. Adsorption isotherm models: A comprehensive and systematic review. *Sci. Total Environ.* **2022**, *812*, 151334. [CrossRef]
50. Nethaji, S.; Sivasamy, A.; Mandal, A.B. Adsorption isotherms, kinetics and mechanism for the adsorption of cationic and anionic dyes onto carbonaceous particles prepared from *Juglans regia* shell biomass. *Int. J. Environ. Sci. Technol.* **2013**, *10*, 231–242. [CrossRef]
51. Flores-Garnica, J.G.; Morales-Barrera, L.; Pineda-Camacho, G.; Cristiani-Urbina, E. Biosorption of Ni(II) from aqueous solutions by *Litchi chinensis* seeds. *Bioresour. Technol.* **2013**, *136*, 635–643. [CrossRef]

52. Quintelas, C.; Rocha, Z.; Silva, B.; Fonseca, B.; Figueiredo, H.; Tavares, T. Removal of Cd(II), Cr(VI), Fe(III) and Ni(II) from aqueous solutions by an *E. coli* biofilm supported on kaolin. *Chem. Eng. J.* **2009**, *149*, 319–324. [CrossRef]
53. Şengil, İ.A.; Özacar, M. Competitive biosorption of $Pb^{2+}$, $Cu^{2+}$ and $Zn^{2+}$ ions from aqueous solutions onto valonia tannin resin. *J. Hazard. Mater.* **2009**, *166*, 1488–1494. [CrossRef]
54. Pipíška, M.; Horník, M.; Vrtoch, L.; Augustín, J.; Lesný, J. Biosorption of Zn and Co ions by *Evernia prunastri* from single and binary metal solutions. *Chem. Ecol.* **2008**, *24*, 181–190. [CrossRef]
55. Kaduková, J.; Horváthová, H. Biosorption of copper, zinc and nickel from multi-ions solutions. *Nova Biotechnol. Chim.* **2012**, *11*, 125–132. [CrossRef]
56. Bolat, Y.; Bilgin, S.; Günlü, A.; Izci, L.; Koca, S.B.; Çetinkaya, S.; Koca, H.H. Chitin-chitosan yield of freshwater crab (*Potamon potamios*, Olivier 1804) shell. *Pak. Vet. J.* **2012**, *30*, 227–231.
57. Youn, D.K.; No, H.K.; Prinyawiwatkul, W. Physicochemical and functional properties of chitosans prepared from shells of crabs harvested in three different years. *Carbohydr. Polym.* **2009**, *78*, 41–45. [CrossRef]
58. Shahidi, F.; Synowiecki, J. Isolation and characterization of nutrients and value-added products from snow crab (*Chionoecetes opilio)* and shrimp (*Pandalus borealis*) processing discards. *J. Agric. Food Chem.* **1992**, *39*, 1527–1532. [CrossRef]
59. Naczk, M.; Williams, J.; Brennan, K.; Liyanapathirana, C.; Shahidi, F. Compositional characteristics of green crab (*Carcinus maenas*). *Food Chem.* **2004**, *88*, 429–434. [CrossRef]
60. Heredia, A.; Aguilar-Franco, M.; Magaña, C.; Flores, C.; Piña, C.; Velázquez, R.; Schäffer, T.E.; Bucio, L.; Basiuk, V.A. Structure and interactions of calcite spherulites with α-chitin in the brown shrimp (*Penaeus aztecus*) shell. *Mater. Sci. Eng. C* **2007**, *27*, 8–13. [CrossRef]
61. Duarte, M.L.; Ferreira, M.C.; Marvão, M.R.; Rocha, J. An optimised method to determine the degree of acetylation of chitin and chitosan by FTIR spectroscopy. *Int. J. Biol. Macromol.* **2002**, *31*, 1–8. [CrossRef]
62. Stuart, B.H. *Infrared Spectroscopy: Fundamentals and Applications*; John Wiley & Sons Ltd.: Chichester, UK, 2004.
63. Naja, G.; Mustin, C.; Volesky, B.; Berthelin, J. A high-resolution titrator: A new approach to studying binding sites of microbial biosorbents. *Water Res.* **2005**, *39*, 579–588. [CrossRef]
64. Beil, S.; Schamberger, A.; Naumann, W.; Machill, S.; van Pée, K.-H. Determination of the degree of N-acetylation (DA) of chitin and chitosan in the presence of water by first derivative ATR FTIR spectroscopy. *Carb. Polym.* **2012**, *87*, 117–122. [CrossRef]
65. Mungasavalli, D.P.; Viraraghavan, T.; Jin, Y.-C. Biosorption of chromium from aqueous solutions by pretreated *Aspergillus niger:* Batch and column studies. *Colloid Surf. A-Physicochem. Eng. Asp.* **2007**, *301*, 214–223. [CrossRef]
66. Lee, M.-Y.; Park, J.M.; Yang, J.-W. Micro precipitation of lead on the surface of crab shell particles. *Process Biochem.* **1997**, *32*, 671–677. [CrossRef]
67. Londono-Zuluaga, C.; Jameel, H.; Gonzalez, R.W.; Lucia, L. Crustacean shell-based biosorption water remediation platforms: Status and perspectives. *J. Environ. Manag.* **2019**, *231*, 757–762. [CrossRef] [PubMed]
68. Jeon, D.J.; Yeom, S.H. Recycling wasted biomaterial, crab shells, as an adsorbent for the removal of high concentration of phosphate. *Bioresour. Technol.* **2009**, *100*, 2646–2649. [CrossRef] [PubMed]